Three-Dimensional Self-Assembled Hierarchical Architectures of Gamma-Phase Flowerlike Bismuth Oxide

Teng-Kuan Tseng,*,† Jihun Choi,† Doh-Won Jung,†,‡ Mark Davidson,†,§ and Paul H. Holloway†,§

Department of Materials Science and Engineering and MICROFABRITECH, University of Florida, Gainesville, Florida 32611-6400, and Samsung Advanced Institute of Technology, #14-1, Nongseo-dong, Yongin-si 446-712, Korea

ABSTRACT Three-dimensional (3D) self-assembled hierarchical bismuth oxide architectures were prepared via a solution precipitation synthesis at 85 °C in 45 min with the aid of polyethylene glycol-8000 (PEG-8000) as a capping agent. The morphology and crystalline phase evolution was studied versus reaction time and capping agent concentration and interpreted in terms of growth mechanisms. At higher capping agent concentrations, the as-grown 3D hierarchical flowerlike bismuth oxide was crystalline cubic γ-phase that was previously formed only at temperature ≥640 °C. The morphology and crystal structure of these 3D cubic γ-phase bismuth oxide flowers were not changed with calcining up to 600 °C. Photoluminescence was attributed to emission from the Bi^{3+} ion by a $^3P_{0,1} \rightarrow {}^1S_0$ transition and from defects. The γ-phase flowerlike bismuth oxide shows better ion conductivity than that of rodlike bismuth oxide formed without the capping agent. The flowerlike morphology was attributed to modification of the nucleation and growth kinetics by the capping agent.

KEYWORDS: hierarchical architectures • bismuth oxides • capping agent • self-assembled • photoluminescence • ionic conductivity

INTRODUCTION

A number of applications of bismuth oxide have been widely studied, including optical coating, gas sensor, solid-state electrolytes, microelectronics, and electroceramic, because of its opto-electronic, catalyst, photoluminescence, and ion-conducting properties (1−5). Bismuth oxide is a complex material with four main polymorphs that are denoted by α- (monoclinic), β- (tetragonal), γ- (body-centered cubic), and δ-Bi_2O_3 (face-centered cubic), along with a new modification, ε-bismuth oxide (6). Each polymorph is characterized with distinct structural, optical and electrical properties. The α and δ phases are the stable phases at room temperature and high temperature (between 729 °C and the melting point at 824 °C), respectively. The others are high-temperature metastable phases and usually transform into the stable monoclinic α-Bi_2O_3 (7, 8). Among them, δ-Bi_2O_3 has the best known oxide ion conductivity which makes it appealing for fuel cell and sensor applications, but its narrow stable temperature range of 729−824 °C along with cracking and deterioration during phase transitions limits its use. The addition of rare-earth dopants can stabilize the cubic phase, but the conductivity drops by two orders of magnitude and stability remains an issue. Several studies have been reported on the synthesis of α-Bi_2O_3 in the form of spheres or one-dimensional structure using techniques such as chemical bath deposition (CBD), electrospinning, hydrothermal synthesis, flame spray pyrolysis (FSP), and microemulsion methods (9−13). In addition, δ-Bi_2O_3 has been synthesized by epitaxial electrodeposition onto cubic Au single-crystal substrates or by introducing VO_3^- into the reaction system (1, 14). However, there are no reports of γ-phase Bi_2O_3 having been synthesized at low temperatures in short reaction times without subsequent heat treatment. Several methods have been reported for the synthesis of Bi_2O_3 nanoparticles, nanowires, nanotube, nanofibers and nanohooks (12, 13, 15−17), but there are only a few reports on the synthesis of three-dimensional (3D) hierarchical structures. To date, strategies for synthesis of these materials with higher dimension structures under template-free and cost-effective conditions remain a challenge. In this work, 3D flowerlike γ-Bi_2O_3, composed of 2D building blocks, was synthesized via a facile solution precipitation method using low reaction temperatures and short times with the aid of polyethylene glycol-8000 (PEG-8000). Structural, photoluminescence, and conductivity properties of hierarchical γ-Bi_2O_3 are reported.

EXPERIMENTAL SECTION

All chemicals were analytical grade and used as received without further treatment. The typical solution precipitation procedure was begun by dissolving 1.94 g of $Bi(NO_3)_5H_2O$ in 20 mL of HNO_3 (1 M) to form a clear solution, followed by adding 200 mL of deionized water. The precursor mixture was heated to 85 °C and different concentrations of PEG-8000

* Corresponding author. E-mail: ttkuan@gmail.com.
Received for review November 21, 2009 and accepted March 10, 2010
† Department of Materials Science and Engineering, University of Florida.
‡ Samsung Advanced Institute of Technology.
§ MICROFABRITECH, University of Florida.
DOI: 10.1021/am900812a

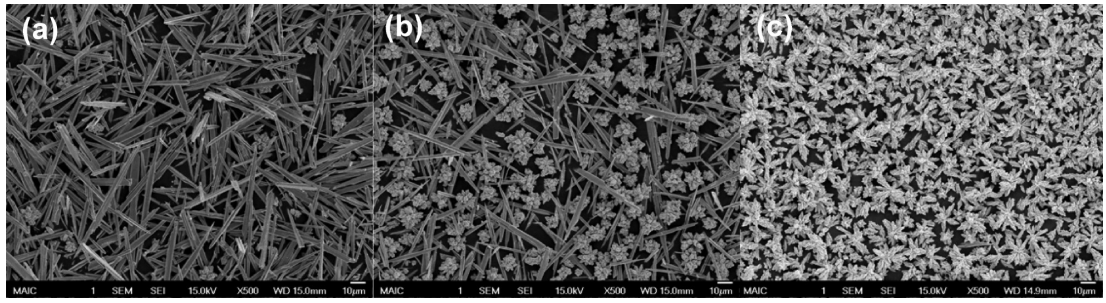

FIGURE 1. SEM images of morphology evolution as a function of PEG-8000 volume fraction, C = (a) 0.05, (b) 0.1, and (c) 0.2 (reaction temperature = 85 °C, time = 45 min).

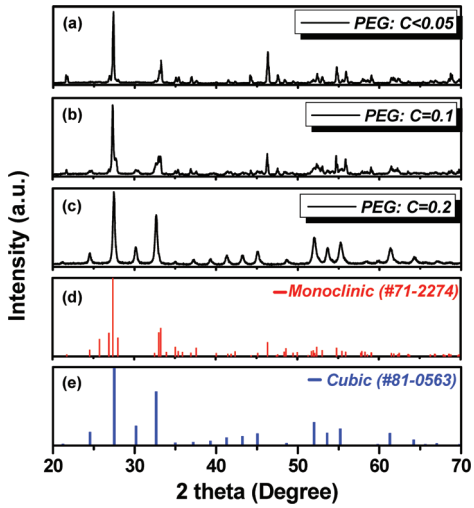

FIGURE 2. X-ray diffraction (XRD) pattern for bismuth oxide as a function of PEG-8000 volume fraction, C = (a) 0.05, (b) 0.1, and (c) 0.2 (reaction temperature = 85 °C, time = 45 min). (d) Diffraction peaks from JCPDS for monoclinic α-bismuth oxide. (e) Diffraction peaks from JCPDS for cubic γ-bismuth oxide.

(designated as "C" and defined as the volume ratio of PEG-8000 to the total precursor solution) was added to the solution with vigorously stirring until a homogeneous clear solution was again obtained. Then 60 mL of NaOH (4M) solution was added to the precursor mixture with continuous stirring to generate a colloidal solution. After various reaction times, the precipitate was collected by washing with DI water and centrifuging several times, followed by oven-drying at 80 °C for 2 h. As-prepared and calcined (600 °C for 2 h in air) samples were characterized by X-ray diffraction (XRD) (Philips APD 3720) with Cu K_α radiation (λ = 1.5418 Å). The XRD pattern was collected from dried powder samples in a step scan (0.02° per step) mode with a small grazing incident angle (~2°) over a 2θ scan range of 20−70°. The morphology and size of Bi_2O_3 were determined with high-resolution transmission electron microscopy (HR-TEM; JEOL 2010F) and with field-emission scanning electron microscopy (FE-SEM; JEOL 6335F). Photoluminescence (PL) and photoluminescence excitation (PLE) spectra were measured at room temperature using a JASCO FP-6500/6600 spectrophotometer with a 150 W xenon lamp. Conductivity was determined by two-point probe electrochemical impedance spectroscopy (EIS) using a Solartron 1260 over the frequency range of 1 Hz to 1 MHz and between 300 and 600 °C in air.

RESULTS AND DISCUSSION

To determine the effects of a surface capping agent on crystal growth and morphology, we added different volume concentrations of PEG-8000 to the precursor solution with other experimental parameters held constant. SEM micrographs show that the morphology of Bi_2O_3 was changed significantly by increased PEG concentration (Figure 1). The morphology was microrods when either zero or low concentrations of PEG-8000 ($C \leq 0.05$) were used, as shown in Figure 1a. With an increased volume concentration of PEG-8000 (C = 0.1 or 0.2), the morphology evolved from microrods into flowerlike crystals (Figure 1b,c, respectively). On the basis of the Gibbs−Curie−Wulff theorem, the morphology can be explained by the relative growth kinetics of different facets of the crysta l (18, 19). Introduction of a capping agent into the reaction can tailor the growth kinetics by modulating the relative free energies of various crystallographic facets. A similar growth mechanism was proposed to explain the growth of ZnO nanocones and FeCo nanocubes in the presence of PEG (20, 21).

Figure 2 shows the XRD spectra as a function of PEG-8000 volume concentration, which indicates that the two distinct morphologies are associated with different crystal structures. The spectrum in Figure 2a indicates that the micro-rods formed at $C \leq 0.05$ are monoclinic α-phase (JCPDS card 71-2274; Figure 2d). However, when the vol-

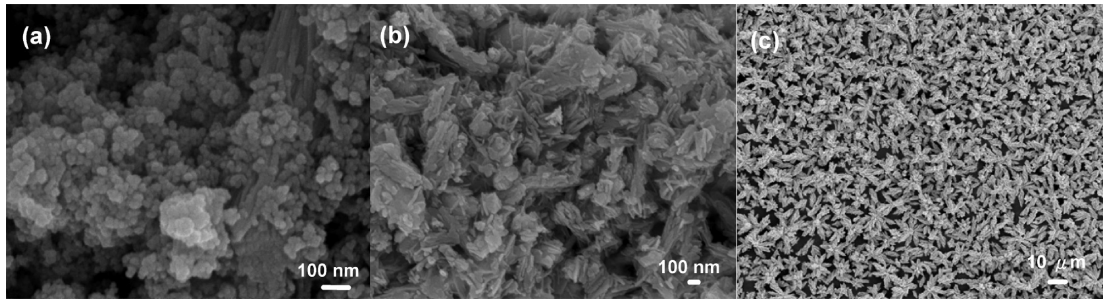

FIGURE 3. Evolution of the morphology of bismuth oxide as a function of reaction times of (a) 1, (b) 10, and (c) 45 min (C = 0.2, reaction temperature = 85 °C).

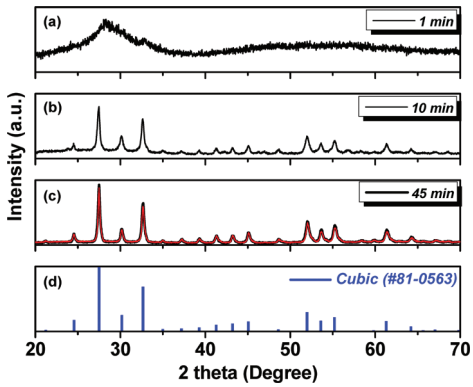

FIGURE 4. XRD pattern from bismuth oxide as a function of reaction times of (a) 1, (b) 10, and (c) 45 min (black, as-grown; red, calcined at 600 °C for 2 h in air; $C = 0.2$, reaction temperature = 85 °C). (d) Diffraction peaks from JCPDS for cubic γ-bismuth oxide.

ume concentration of PEG-8000 was increased to $C = 0.1$ and then to 0.2, the diffraction patterns in Figure 2b,c were from both the monoclinic α and body-centered cubic γ phases, but γ was dominant for the flowerlike morphology from C = 0.2 (JCPDS card 81-0563; Figure 2e). Previously, γ-Bi_2O_3 was reported to form at temperatures of ~640 °C or higher (7).

To investigate the morphology evolution and formation mechanisms of the 3D self-assembled hierarchical architecture, a growth−time analysis was performed with XRD and SEM. The morphology and size of the 3D flowerlike bismuth oxide structure as a function of reaction time from 1 min to 45 min (reaction temperature = 85 °C, $C = 0.2$) are shown by the SEM micrographs in Figure 3. The morphology evolved from ~60 nm nanospheres after 1 min reaction time (Figure 3a), to agglomerated submicrometer clusters after 10 min (Figure 3b), to predominantly 3D flowers after 45 min (Figure 3c). Figure 4 shows the XRD spectra from as-prepared samples for reaction times from 1 to 45 min. Figure 4a shows a broad peak with a large full width at half maximum (FWHM) that is attributed to amorphous nanosized grains. The XRD patterns for reaction times of 10 and 45 min are shown in panels b and c in Figure 4, respectively. Two XRD spectra are shown in Figure 4c, with the black spectrum being from a sample grown for 45 min, and the red spectrum from a sample grown for 45 min then calcined at 600 °C in air for 2 h. Both the as-prepared (black) and calcined samples (red) show a strong crystalline pattern matched by the γ-$Bi_{12.8}O_{19.2}$ phase (i.e., γ-Bi_2O_3), which is composed of umbrellalike [BiO_3] groups and void tetrahedral (JCPDS 81-0563; Figure 4d). In addition, the morphology was not changed by calcining (see Figure S1 in the Supporting Information).

These 3D bismuth flowers have high hierarchy with petals that are composed of self-assembled nano-triangular and pyramid structures as shown in Figure 5a. The typical size of these individual nano-triangles are 600−800 nm. The nano-triangles form a petal which originates from a single center to exhibit the flowerlike geometry. The size of an assembled flower structure is ~10 μm. Figure 5b shows a high-resolution TEM image of a bismuth oxide nano-triangle revealing well-resolved lattice fringes with an interplanar spacing of 0.256 nm. In addition, the selected area electron diffraction (SAED) pattern in the inset of Figure 5b shows single-crystal spots from the cubic γ-phase, consistent with the XRD patterns. Figure 5c shows a room-temperature photoluminescence (PL) spectrum from γ-phase as-prepared flowerlike Bi_2O_3 (excited at 230 nm). The PL spectrum shows broad emission (~400−650 nm) with a peak at ~465 nm due to Bi^{3+} luminescence from the $^3P_0$ and $^3P_1$ excited states to the $^1S_0$ ground state. The green peak at ~562 nm is from an impurity trap associated with oxygen vacancies interacting with interfacial bismuth vacancies (16, 17). The PL transition observed depends on the charge on the bismuth ion, and the blue and green emissions are consistent with trivalent bismuth ions.

The ion conductivities of α-phase microrods and γ-phase flowerlike Bi_2O_3 shown in Figure 6 were determined using impedance spectroscopy. The activation energy can be obtained from the Arrhenius equation by plotting the conductivity, σ, as a function of inverse temperature, T^{-1}

$$\sigma = A\exp\left(-\frac{E_a}{kT}\right) \quad (1)$$

where A is the pre-exponential factor, E_a is the activation energy, and k is Boltzman's constant. The activation energies determined from Figure 6 are 1.07 and 0.54 eV for rod- and flowerlike Bi_2O_3, respectively. Note that the calcined ion conductivity of flowerlike Bi_2O_3 is higher than that of rodlike Bi_2O_3 by a temperature-dependent factor ranging from ~2 at 600 °C to ~32 at 350 °C. The values of the conductivity of γ-phase Bi_2O_3 at temperatures <520 °C have not been reported, but the data in Figure 6 suggest that operation of a fuel cell at these lower temperatures should be feasible.

In general, the crystalline phase, particle size, and morphology of a solid depend strongly on the competition between nucleation and growth, the rates of which are determined by the chemical potentials in the precursor solution. During the initial reaction, bismuth oxide probably nucleated as the reagent acid was poured into the precursor solution, and grew to nanosized particles in < 1 min. With continued reaction, nanosized particles were oriented and attached to other nanoparticles, leading to agglomerated nanoparticles that serve as crystal seeds to grow the flowerlike structure. PEG-8000 is an amphipathic nonionic surface active agent from oxyethylene polymerization, and therefore a PEG−OH bond should form in aqueous solution and chelate bismuth ions, which would lead to highly mobile molecules with a large exclusion volume. The PEG chains result in the morphology of the initially formed bismuth oxide clusters. Moreover, because of the large amount of high-molecular-weight PEG-8000, the precursor solution is viscous leading to the agglomeration of nano-size bismuth oxide clusters to form submicrometer-triangular platelets. Finally, PEG-8000 leads to bridging flocculation, which binds triangular platelets into individual petal-like structures, resulting in flowerlike γ-Bi_2O_3.

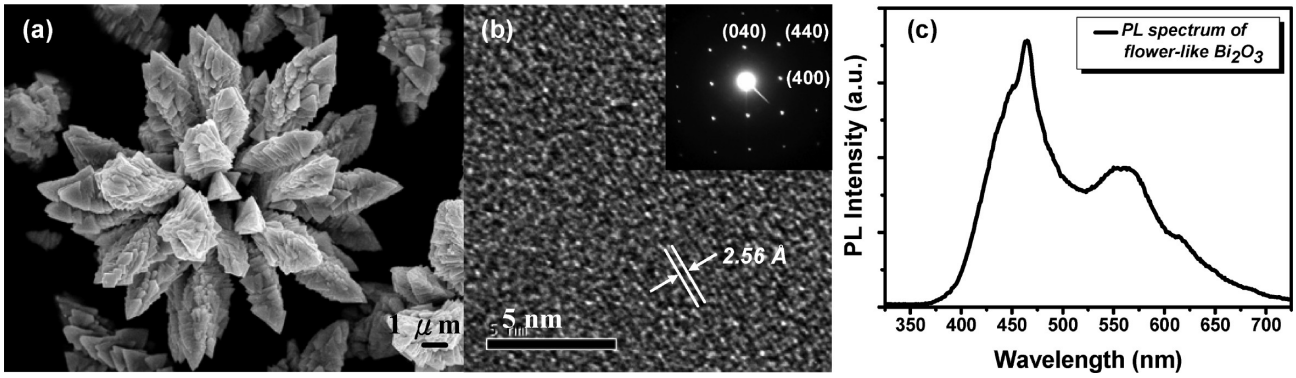

FIGURE 5. (a) SEM micrograph of an individual "flower" of bismuth oxide. (b) TEM micrograph of the lattice fringes from an individual nanotriangle with its' SAED pattern shown in the inset. (c) Photoluminescence spectrum of as-synthesized flowerlike γ-bismuth oxide for excitation at 230 nm.

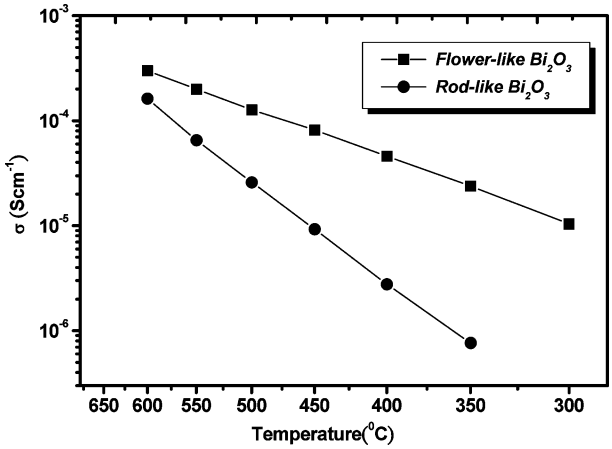

FIGURE 6. Ionic conductivities versus 1/T for rodlike α- and flowerlike γ-bismuth oxide.

SUMMARY

Unique hierarchical 3D self-assembled flowerlike γ-Bi_2O_3 was produced in the presence of PEG-8000 via a facile solution precipitation process without any templates. This is the first report of the growth of body-centered cubic γ-phase Bi_2O_3 at such a low temperature (85 °C) and a short time (45 min). By varying the reaction time and PEG-8000 capping agent concentration, we investigated the evolution of morphology and crystal phase of bismuth oxide. The present data show that the γ-phase Bi_2O_3 formed at 85 °C is stable up to at least 600 °C. The photoluminescent properties and possible growth mechanisms were discussed. The ionic conductivities of the flowerlike γ-Bi_2O_3 and rodlike α-Bi_2O_3 for temperatures between 350 and 600 °C were reported, and flowerlike γ-Bi_2O_3 showed better ion conductivity than did rodlike α-Bi_2O_3.

Acknowledgment. This work was supported by Defense of Threat Reduction Agency (DTRA) Grant No. HDTRA1-08-1-0015. The support by Kerry Siebein of the Major Analytical Instrumentation Center and use of equipment in the Particle Engineering Research Center at the University of Florida are gratefully acknowledged.

Supporting Information Available: SEM photomicrographs of hierarchical flowerlike γ-Bi_2O_3 after calcining at 600 °C for 2 h in air showing no change in morphology (PDF). This material is available free of charge via the internet at http://pubs.acs.org.

REFERENCES AND NOTES

(1) Switzer, J.; Shumsky, M.; Bohannan, E. *Science* **1999**, *284*, 293–296.
(2) Chris, E.; Svein, S.; Stefan, T.; Stephen, H. *Phys. Rev. Lett.* **2009**, *102*, 155502–155506.
(3) Laurent, K.; Wang, G.; Tusseau-Nenez, S.; Leprince-Wang, Y. *Solid State Ionics* **2008**, *178*, 1735–1739.
(4) Leontie, L.; Caraman, M.; Alexe, M.; Harnagea, C. *Surf. Sci.* **2002**, *507—510*, 480–485.
(5) Sugimoto, N. *J. Ceram. Soc. Jpn.* **2008**, *116*, 1028–1032.
(6) Cornei, N.; Tancret, N.; Abraham, F.; Mentre, O. *Inorg. Chem.* **2006**, *45*, 4886–4888.
(7) Harwig, A.; Gerards, G. *J. Solid State Chem.* **1978**, *26*, 265–274.
(8) Mehring, M. *Coord. Chem. Rev.* **2007**, *251*, 974–1006.
(9) Gujar, T.; Shinde, V.; Lokhande, C.; Mane, R.; Han, S.-H. *Appl. Surf. Sci.* **2005**, *250*, 161–167.
(10) Kim, H. W.; Lee, J. W.; Shim, S. H. *Sens. Actuators, B* **2007**, *126*, 306–310.
(11) Yang, Q.; Li, Y.; Yin, Q.; Wang, P.; Cheng, Y.-B. *Mater. Lett.* **2002**, *55*, 46–49.
(12) Wang, C.; Shao, C.; Wang, L.; Zhang, L.; Li, X.; Liu, Y. *J. Colloid Interface Sci.* **2009**, *333*, 242–248.
(13) Dong, W.; Zhu, C. *J. Phys. Chem. Solids* **2003**, *64*, 265–271.
(14) Zhou, L.; Wang, W.; Xu, H.; Sun, S.; Shang, M. *Chem.—Eur. J.* **2009**, *15*, 1776–1782.
(15) Jungk, H.-O.; Feldmann, C. *J. Mater. Sci.* **2001**, *36*, 297–299.
(16) Lee, D.; Hong, S. *J. Korean Phys. Soc.* **2008**, *53*, 1965–1970.
(17) Kumari, L.; Lin, J.-H.; Ma, Y.-R. *J. Phys.: Condens. Matter* **2007**, *19*, 406204–406215.
(18) Sun, Y.; Xia, Y. *Science* **2002**, *298*, 2176–2179.
(19) Xia, Y.; Yang, P.; Sun, Y.; Wu, Y.; Mayers, B.; Gates, B.; Yin, Y.; Kim, F.; Yan, H. *Adv. Mater.* **2003**, *15*, 353–389.
(20) Wei, X.; Zhu, G.; Liu, Y.; Ni, Y.; Song, Y.; Xu, Z. *Chem. Mater.* **2008**, *20*, 6248–6253.
(21) Cheng, C.; Xu, G.; Zhang, H.; Luo, Y.; Zhang, P.; Shen, K. *Mater. Res. Bull.* **2008**, *43*, 3506–3513.

AM900812A